Ann. Occup. Hyg., Vol. 54, No. 6, pp. 615–624, 2010

doi:10.1093/annhyg/meq053

Characterization of Nanoparticle Release from Surface Coatings by the Simulation of a Sanding Process

DANIEL GÖHLER, MICHAEL STINTZ*, LARS HILLEMANN and MANUEL VORBAU

Research Group Mechanical Process Engineering, Institute of Process Engineering and Environmental Technology, Technische Universität Dresden, D-01062 Dresden, Germany

Received 22 February 2010; in final form 14 June 2010; published online 2 August 2010

Nanoparticles are used in industrial and domestic applications to control customized product properties. But there are several uncertainties concerning possible hazard to health safety and environment. Hence, it is necessary to search for methods to analyze the particle release from typical application processes. Based on a survey of commercial sanding machines, the relevant sanding process parameters were employed for the design of a miniature sanding test setup in a particle-free environment for the quantification of the nanoparticle release into air from surface coatings. The released particles were moved by a defined airflow to a fast mobility particle sizer and other aerosol measurement equipment to enable the determination of released particle numbers additionally to the particle size distribution. First, results revealed a strong impact of the coating material on the swarf mass and the number of released particles.

Keywords: abrasion process; exposure; nanoparticle additives; nanoparticle release; sanding process; surface coatings

INTRODUCTION

Nanoparticles are used in industrial and domestic applications to control customized product properties. For instance, in the area of surface coatings, nanoparticle-based additives improve scratch resistance, ultraviolet light resistance or transparency for visible light (e.g. Sepeur *et al.*, 1999; Gläsel *et al.*, 2000; Bauer *et al.*, 2002). But there are several uncertainties concerning possible hazard to health safety (e.g. Lam *et al.*, 2004; Singh *et al.*, 2009) and environment (e.g. Karn *et al.*, 2009). Up to now, there are no standardized methods for the characterization of the nanoparticle release from surfaces in dependency on certain treatment processes. One objective of this study are methodical findings concerning the necessary treatment and measurement conditions, to be specified for comparability of tests and future standardization, similar to the actual standardization project ISO/DIS 12025.

In a previous study, a common domestic treatment like walking with scratching shoes on parquet coatings was simulated by using the Taber Abraser Test (Vorbau *et al.*, 2009). This method bases on a weak but long-term abrasion with sanding wheels. Normally, the material release is measured by weighing the sample before and after the treatment. Measurements with a scanning mobility particle sizer (SMPS) and a condensation particle counter (CPC) have shown no significant nanoparticle release. In this slow abrasion treatment test, only particles in the micrometer size range were detected.

Hsu and Chein (2007) designed an experimental setup for simulating the abrasive effect of sunlight, wind, and human contact by using ultraviolet lamps, a fan, and a rubber in a closed chamber, respectively. Coatings with TiO_2 nanoparticle additives on wood,

*Author to whom correspondence should be addressed.
Tel: +49-351-46335176; fax: +49-351-46337058;
e-mail: michael.stintz@tu-dresden.de

polymer, and tile were analyzed in a size range between 15 and 661 nm using an SMPS. The TiO_2 coating on the tile was found to have the highest particle emissions. Hsu and Chein assume that the investigated actions greatly reduce the adhesion forces between the primary TiO_2 particles and the carrier surface and, therefore, result in particle emissions from the coating products.

Investigations to characterize the dust and the filtration efficiency due to the sanding of wood using different types of sanders have been made by Thorpe and Brown (1994). The released particles were analyzed using an aerodynamic particle sizer (APS) to measure the particle size distribution in the micrometer size range and a hand-held aerosol monitor and membrane filter elements for determining the dust concentration.

Koponen *et al.* (2009) investigated the particle size distributions of sanding dust released from paints produced with and without engineered nanoparticles. They connected a commercial hand-held orbital sander without filter bag to a stainless steel human exposure chamber (dust reservoir). The dust from the chamber was sampled by a fast mobility particle sizer (FMPS) and an APS. Few millimeter thick layers of paint containing TiO_2 and carbon black nanoparticles were sanded. In the result, five log-normal distributions were fitted to the measured complete particle size distributions between 0.006 μm and 20 μm. Mechanical wear and spark particles from the electrical motor were found to be the main source of particles $<$50 nm, represented by the two smallest log-normal distributions. The modes of the log-normal distributions did not depend on whether nanoparticles were present in the paints or not, but the modal number concentrations varied among the different paints.

Based on a survey of commercial sanding machines, the relevant abrasion process parameters (contact pressure and peripheral speed) were used to design the sanding test setup in laboratory scale for the present work. The experimental setup operated in a laminar flow box and directed the sander exhaust flow to the laminar flow box exit. Thus, the entrance of nanoparticles from the electrical motor and the environment to the swarf aerosol sample was excluded.

EXPERIMENTAL DETAILS

Sanding process

For a defined sanding of surface coatings, a miniature sander (Model Dremel 400 Series Digital; Dremel Europe, Breda, The Netherlands) was used. The sander consists of one abrasion wheel (diameter of 7 mm) that rotates with an adjustable peripheral speed in the range of 1.8–24 $m \cdot s^{-1}$. The sanding process is caused by the contact between the sample surface and the abrasion wheel. A variation of abrasiveness can be attained by changing the grain size of the abrasive paper on the abrasion wheel (graining of 600), the contact force, and therefore the contact pressure or the rotational speed. The sanded surface is a rectangular area of 13 cm^2 and the abrasion material has to be removed continuously with an exhaust device, which is not provided originally.

A defined and standardized stress, which acts on the sample surface, is important for reproducible measurement results. The stress of the sander can be adjusted corresponding to the typical stress applied to the surface coatings in a professional sanding process. The parameters, which have to be specified for the testing method, are the material of the abrasion wheel, the contact force or the contact pressure, and the peripheral speed. The operating parameters of the sander should be similar to an industrial sanding process but are limited by the specification of the particle measurement system. A comparison of the characteristic parameters between the used sander and typical industrial sanding processes is shown in Table 1, based on the technical data of three typical sanding instruments. It can be seen that the employed sander can simulate an industrial sanding process, concerning the contact pressure and the peripheral speed.

Measuring methods

The characterization of the released particles due to the sanding process requires the determination of the particle number concentration and the particle size distribution. Therefore, the aerosol generation section was combined with an aerosol measurement

Table 1. Comparison of characteristic values between the employed miniature sander Dremel and the professional sanding process

	Sander (Dremel)	Typical sanding process
Contact force (N)	$2.0 \times 10^{-1} - 1.0 \times 10^{0}$	$4.0 \times 10^{2} - 4.0 \times 10^{4}$
Contact pressure (Pa)	$1.0 \times 10^{4} - 5.0 \times 10^{4}$	$3.0 \times 10^{3} - 2.0 \times 10^{4}$
Peripheral speed ($m\ s^{-1}$)	1.8–24	3.0–17.0

section. Three instruments were employed in the experimental setup: an FMPS (Model 3091; TSI Incorporated, Shoreview, MN, USA), a laser aerosol particle size spectrometer (LAP; Model LAP 321; Topas GmbH, Dresden, Germany) for determining the number-weighted particle size distribution, and a CPC (Model 3022; TSI Incorporated) for determining the particle number concentration.

The measurement principle of the employed CPC is based on magnifying particles by condensation in a supersaturated atmosphere of *n*-butanol (e.g. Agarwal and Sem, 1980; Sem, 2002). Thus, the aerosol particles can be counted in a size range of 6 nm to a few micrometers at a flow rate of 0.3 $l \cdot min^{-1}$.

The FMPS is an electrical aerosol spectrometer (e.g. Mirme and Peil, 1983; Graskow, 2001; Tammet *et al.*, 2002; Biskos *et al.*, 2005) and determines the particle size distribution with a 1-s resolution in a size range between 5.6 and 560 nm of the aerosol, offering a total of 32 channels of resolution (16 channels per decade). The FMPS operates at a flow rate of 10 $l \cdot min^{-1}$.

For the determination of the particle size distribution in the size range between 0.3 and 30 µm, the laser aerosol particle size spectrometer (LAP) was used (e.g. Baron and Willeke, 2001). The LAP operates at a flow rate of 3 $l \cdot min^{-1}$.

An electrostatic precipitator (ESP) was employed for the deposition of the released particles for further analysis by a scanning electron microscope (SEM). It works similar to the nanometer aerosol sampler (Model 3089; TSI Incorporated) and permits the deposition of nanoparticles for a subsequent microscopic analysis (e.g. Hinds, 1999). The particles are charged with a corona charger at a voltage of −3 kV and deposited on a transmission electron microscope (TEM) grid by an electrical field that is operated with a voltage of +13 kV. During the experiments, a volumetric flow rate of 0.3 $l \cdot min^{-1}$ was adjusted.

The requirements of the aerosol measurement techniques had to be matched with the parameters of the sanding process, e.g. by diluting the generated aerosol. In the case of particle concentration $>1 \times 10^4$ cm^{-3}, the particle concentration of the bypass flow to the CPC was diluted using one or two dilution systems (Model VKL 10; Palas GmbH, Karlsruhe, Germany).

All investigations were performed in a particle-free atmosphere maintained with a laminar flow box (Model LF-VM-K0615; Steag Laminarflow Prozesstechnik GmbH, Pliezhausen, Germany). For the purpose of interpretation, the measured particle concentration was calculated to the total number of released particles. The wear rate was determined by weighing the clean sample at the beginning and at the end of the sanding process.

Interconnection of the abrasion process and the aerosol measurement techniques

Figure 1 shows the developed experimental apparatus, which allows to combine high-sensitivity aerosol measurement techniques with a professional sanding process.

The employed sander is mounted on a vertical movable carriage to adjust different contact forces. The sample had to be mounted on the translation sample carrier that moves horizontally beneath the abrasion tool. A radial symmetric sampling hood with a volume of 60 cm^3 provides a complete encapsulation of the sampling suction zone behind the abrasive wheel. The sampling hood avoids particle loss in the laminar flow box. Furthermore, the aerosol concentration remains relatively high due to the low volume of the sampling hood and the total sample flow that amounts to 13.9 $l \cdot min^{-1}$. To prevent particle contamination from the cooling motor fan output (spark particles) of the sander, a blow shield for directing this exhaust flow to the laminar flow box exit was appended.

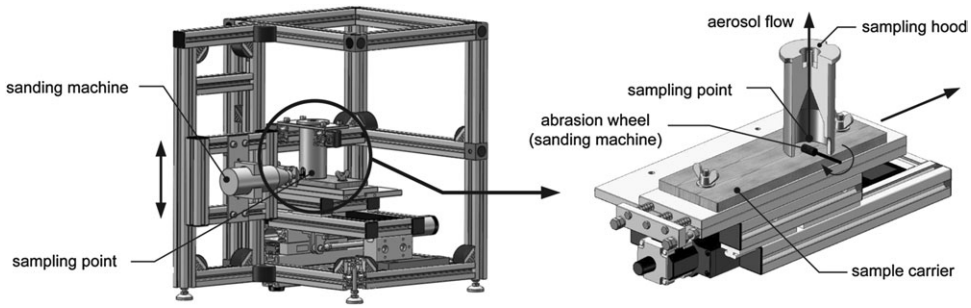

Fig. 1. 3D-CAD-Model of the employed test device with marked sampling hood.

The measurement systems described in section Measuring Methods get their sample flows from a splitter system, which was arranged behind the sampling hood. For each simulation of the sanding process (80 s), a few operating steps have to run. At first, the laminar flow box and the ESP were started, running the whole time. The FMPS, the CPC, and the LAP measurements were started after 10 s for a measurement time of 60 s. The actual abrasion process (duration 20 s at a sample feed rate of 0.3 $m \cdot min^{-1}$) was started after another 10 s. So the sanding process was detected with a lead time of 10 s (for determining the background) and a lag time of 30 s (for collecting all dust particles). The operation time of 20 s was based on optimized experimental conditions to ensure that only the thin layer surface coatings were sanded and not the sample carrier material.

Figure 2 shows a schematic diagram of the whole experimental setup, which was necessary for determining the nanoparticles release due to the sanding process.

Background and reference measurements

A test aerosol was dosed directly in the sampling zone of the abrasion module to verify the suitability of the sampling and measurement system. To determine losses in the size range of the employed nanoparticle additives, a spherical monodisperse latex suspension (Nanosphere Standards; Duke Scientific Corporation, Palo Alto, CA, USA) was chosen for generating a stable test aerosol. The primary aerosol generated by an atomizer (Model ATM 220; Topas GmbH) was first dehumidified using a diffusion dryer unit (Model DDU 570; Topas GmbH); then, it was classified in a differential mobility analyzer (Model 3071; TSI Incorporated), which was operated at a flow ratio of $Q_a/Q_{sh} = 1/4$ [$(l \cdot min^{-1})/(l \cdot min^{-1})$]. This results in a particle size distribution with a relative SD of 0.36. Reference experiments proved number average particle sizes of 80 nm in a concentration of ~4900 cm^{-3}. The experimental relative standard deviation of the measured concentrations of the 80 nm particles remained almost constant (average coefficient of variation 0.012) for three measurements.

In a further step, the background concentration, generated by the running abrasion module without sample contact but with operating the sanding machine, was investigated before the experiments. The average concentration of released particle of ~0.01 cm^{-3} was detected by the CPC with a total average number of 0.2 released particles in an analyzed volume of 300 cm^3. So the abrasion module released practically no significant particle concentration. The background particle concentration was too low for particle size distribution measurements by FMPS.

Surface coating materials

For the characterization of the particle release due to professional sanding processes, two different coatings were chosen and applied on two different carrier materials. Table 2 shows the coating materials that were analyzed during this study.

The samples were prepared according to a standard procedure, which is described in detail in a previous paper (Vorbau *et al.*, 2009). Only the thickness of the surface coatings was increased, for the two-pack polyurethane coating from 21.0 to 41.0 µm and for the white-pigmented architectural coating from 70–110 µm to 130–150 µm. The determination of the thickness of the surface coatings was conducted according to the German standard DIN EN ISO 2178 for the two-pack polyurethane coatings and with a Foil Thickness Gauge (Model 497; Erichsen, Hemer, Germany) for the white-pigmented architectural coatings.

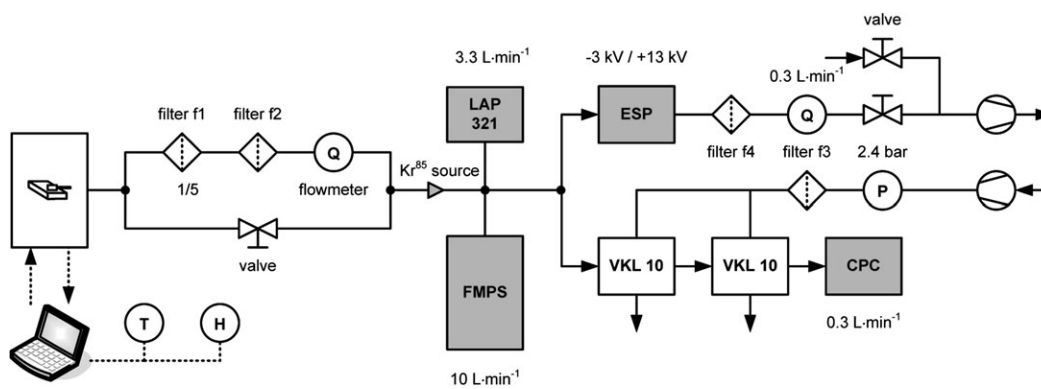

Fig. 2. Schematic diagram of the experimental setup for the nanoparticles release characterization due to the sanding process.

Table 2. Analyzed coating samples and carrier materials

	Sample carrier	Additive	ID
Two-pack polyurethane coating	Steel panel	—	PU
Two-pack polyurethane coating	Steel panel	ZnO	PU-ZnO
White-pigmented architectural coating	Fiber cement plate	—	AC
White-pigmented architectural coating	Fiber cement plate	ZnO	AC-ZnO
White-pigmented architectural coating	Fiber cement plate	Fe_2O_3	AC-Fe_2O_3

In addition to the abrasion test, the particle size distributions of the nanoparticle additives from the coatings were analyzed in suspensions by a photon cross correlation instrument (Nanophox; Sympatec, Clausthal-Zellerfeld, Germany), which primarily detects the diffusion velocity of the particles. The original paint additives were diluted and most agglomerates were dispersed before the measurements.

Figure 3a shows the density functions of the number-weighted particle size distributions of the employed additives while Fig. 3b shows the cumulative particle size distributions.

According to Fig. 3b, the number percentage of particles $<$100 nm of the ZnO additive amounts to 75%, whereas the number percentage of particles $<$100 nm of the Fe_2O_3 additive amounts to 25%. In contrast to the Fe_2O_3 additives (coarse but narrow distributed), the ZnO additives are finer but considerably broader distributed.

RESULTS AND DISCUSSION

For each coating, shown in Table 2, five different samples (i.e. carriers with coating) were examined with the developed experimental setup. After the first run, the sample carrier was turned and abraded a second time. By this way, a total number of 10 aerosol measurements for each coating were achieved. The results of the measurements are depicted in graphs by the average values.

At first, the swarf mass of the samples of every run was determined. Next to them, the total numbers of all released particles into air from the surfaces coatings were quantified with the CPC. Both the swarf mass and the total number of released particles of each sample are compared in Fig. 4.

The swarf mass and the total number of released particles obviously depend on the coating material (compare PU and AC). For PU and PU-ZnO, a slight impact of the dosed nanoparticles is visible as well.

In spite of constant experimental conditions, a significant data spread can be observed; however, the data spread of the swarf mass does not correlate with the data spread of the total number of released particles. For example, the variation of the swarf mass for the AC sample is $\sim$20% and for the total number of released particles is $\sim$70%. The variation of the swarf mass results from random errors of only the abrasion process of material from the coating, whereas the variation of the total number of particles is additionally depending on the random errors of the dispersion process of the abraded swarf material into air, respectively the aerosol size distribution.

Due to the high uncertainty in the experimental data, it is not possible to define any general correlation between the swarf mass and the number of wear particles (i.e. general particle size distribution). In fact, it is more likely that both parameters are related to material-specific properties. An indication of this may be the results of the samples AC, AC-ZnO, and AC-Fe_2O_3, which have high swarf mass and relatively low aerosol number at the same time. This is only explainable with lower mechanical rigidity, causing the higher wear masses of larger wear particle sizes. The airborne particles in micrometer size range were analyzed by the LAP. Coarse particles that remained on the sample surface during a short break of the sample suction airflow were suspended in propanol after the sanding process and analyzed by a single particle optical extinction counter, which works similar to the particle counter for fluids FAS 362 (Topas GmbH).

Figure 5 shows the results of the AC and PU coatings containing and not containing nanoparticle additives. The coarser distribution of AC-Fe_2O_3 swarf in the micrometer size range causes the greater swarf mass of the sample despite the lower number of released particles in comparison to PU-ZnO. The representation of results as density distribution, weighted by volume, allows the interpretation of the area under the curve in a certain size range as a volume percentage or a mass percentage. It shows that mass loss is dominated by particles $>$20 μm, above the aerosol measurement particle size range. On the other hand, the submicrometer range dominates the number release of particles.

The SEM images, which are shown in Fig. 6, confirm these results. The performed SEM and TEM analysis show only wear particles from the coating

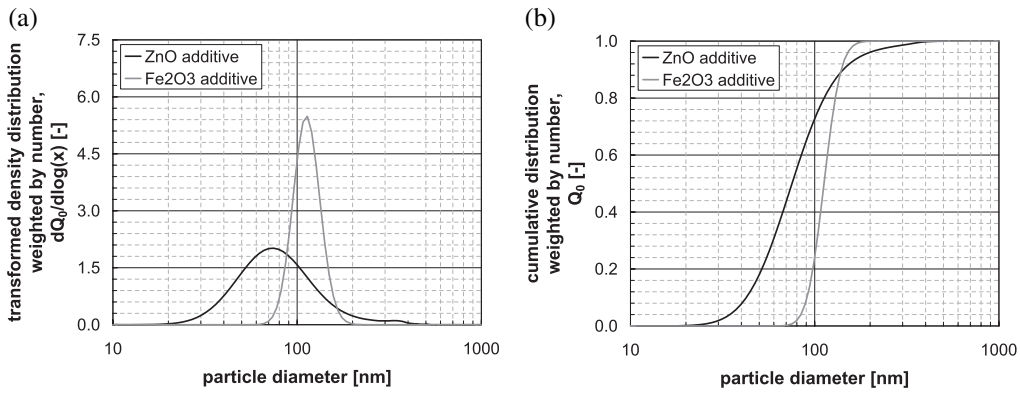

Fig. 3. Number-weighted density (a) and cumulative (b) particle size distributions of the employed nanoparticle additives.

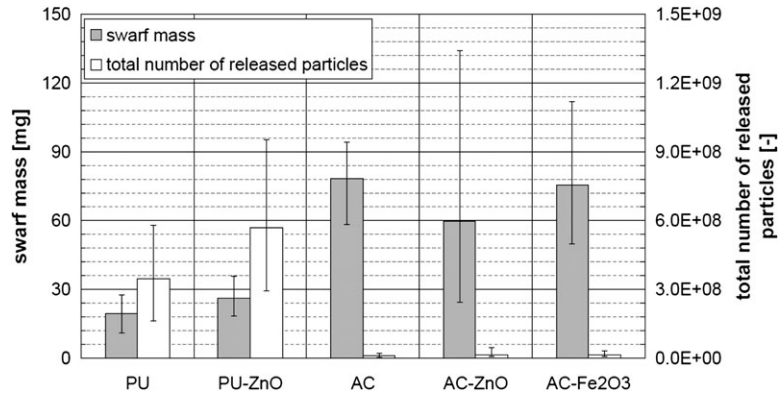

Fig. 4. Total number of released particles in comparison to the swarf mass.

material. Additional analyses of the abrasive paper surface after the sanding process show that no abrasive particles were removed. Therefore, it can be assumed that the abraded surface coating material is the main source for both the fine and the coarse particles.

Further details on the sanding process can be drawn from the FMPS results. The temporal courses of the nanometer particle size distributions for the sample PU and PU-ZnO are illustrated in Fig. 7.

Figure 7 shows that the particle size distribution of the released aerosol from the PU coatings is constant in time. Nevertheless, the number concentration density varies over the investigated time, i.e. over the sanding process, the number of released particles varies but not the particle size distribution. After the beginning of the abrasion process, the number of released particles increases to the maximum and decreases afterward to the initial state. The determined maxima occur at a measurement time of ∼30 s. The modal values of the released particles are in the size range of 90–100 nm.

The particle size distribution is not identical with the distribution in Fig. 8 because of the fewer released particles. The difference in the fine particle size range of the AC coatings results from the increase of the inherent electrometer noise by the decrease of the particle number concentrations. The characteristic peak (compared to PU coatings in Fig. 7), which is significant for the investigated sanding processes, is a little bit coarser than 100 nm. The average number of the total released particles and the average number of released particles <100 nm are illustrated in Fig. 9. The variations of the particle number release over magnitudes require a logarithmical scaling of the ordinate.

The number of released particles depends foremost on the employed coating material. For the PU coating, the released particles are almost exclusively

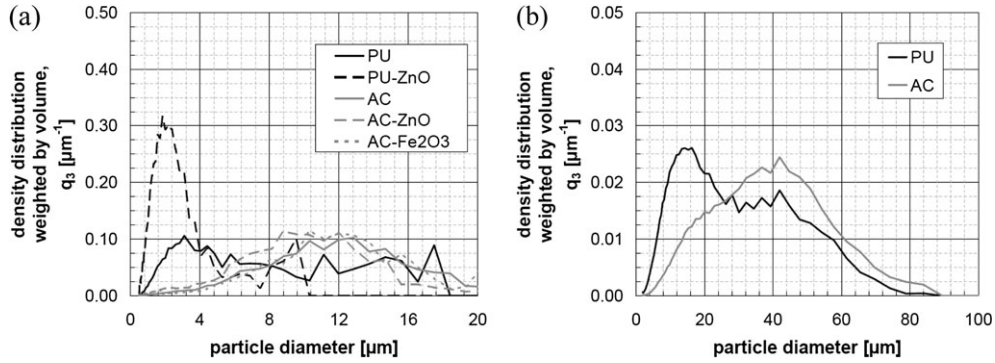

Fig. 5. Particle size distributions, weighted by volume, of (a) the employed coatings swarf aerosol containing and not containing nanoparticle additives and (b) sanding swarf particles after suspension of the collected swarf (AC-Fe_2O_3 and PU-ZnO) in propanol and ultrasonic bath dispersion.

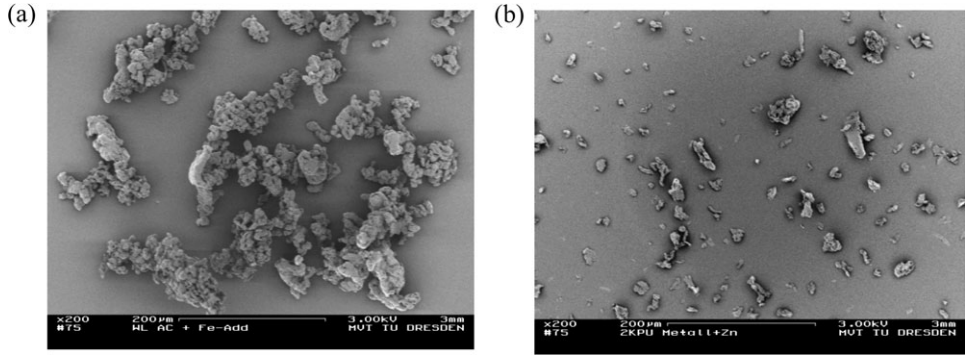

Fig. 6. Sanding swarf of AC-Fe_2O_3 (a) and PU-ZnO (b); size distribution of PU-ZnO is finer and broader; bar size 200 µm.

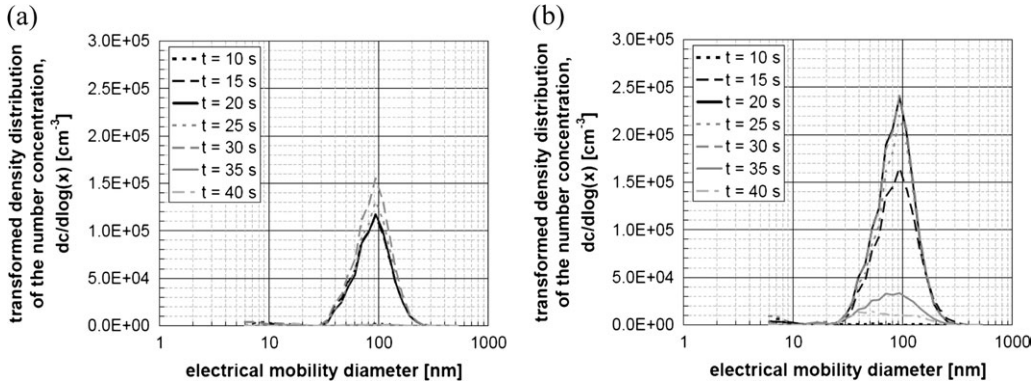

Fig. 7. Evolution of FMPS particle size distributions: (a) PU and (b) PU-ZnO.

<250 nm and approximately half of the released particles are <100 nm (see Fig. 7).

During the abrasion tests, no significant difference was detected between the number concentrations of released particles <100 nm of the pure coatings and of the coatings that were dosed with additives.

One explanation could be the fact that the dosed additives are embedded in the generated wear. This could be confirmed with the SEM and TEM analyses. The dosed nanoparticles are clearly visible within the wear particles and show the characteristic morphology of the dosed additives (zinc oxide or iron oxide). Figure 10 compares the embedded

additive particles of the AC and the PU coating at a magnification of ×50 000. Furthermore, Fig. 11 shows a typical TEM image of one PU-ZnO sample.

The SEM and TEM images clearly prove that the additive particles are still embedded in the wear sample. No free zinc oxide particles could be collected or additionally counted.

Assuming an ideal mixing and neglecting coagulation, the number of released particles in Fig. 9 can be illustrated by introducing a model room as it is employed in clean room techniques (Gail and Hortig, 2004) enclosing the discussed release process. Accordingly, a model room with an area of 10 m^2 and a height of 3 m was applied. Based on the measured data, the nanoparticle release from a 13 cm^2 sanding area varies between 2.4×10^6 and 2.5×10^8. Dependent on the room height, particle number concentrations between 6.15×10^2 cm^{-3}

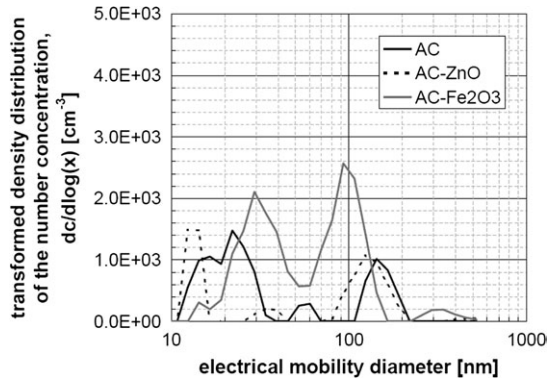

Fig. 8. Characteristic particle size distributions of the AC coatings containing and not containing nanoparticle additives.

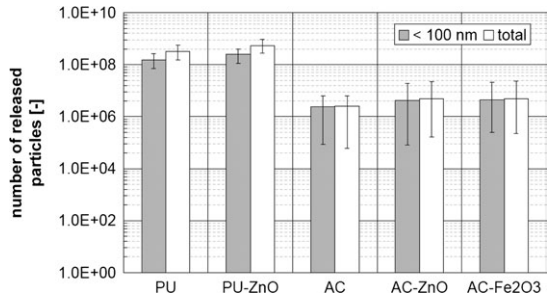

Fig. 9. Average number of total released particles and released particles <100 nm with minimum and maximum spreads, based on a sanding area of 13 cm^2.

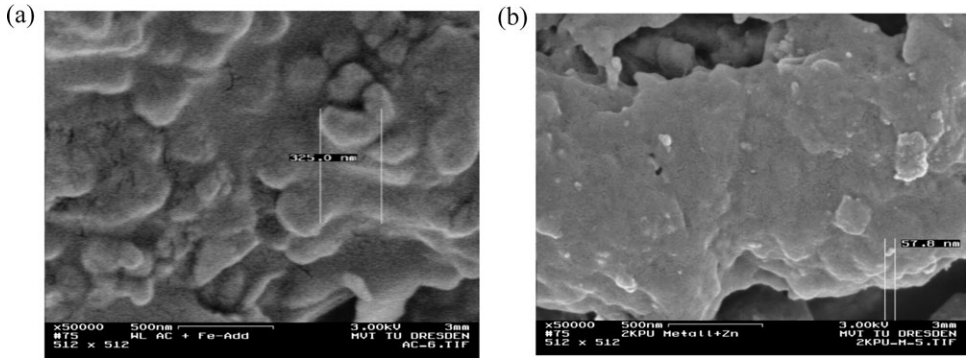

Fig. 10. Embedded pigment particles (e.g. 325 nm) in sanding swarf of AC-Fe_2O_3 (a) and few ZnO-particles embedded below the surface of PU-ZnO swarf (b); bar size 500 nm.

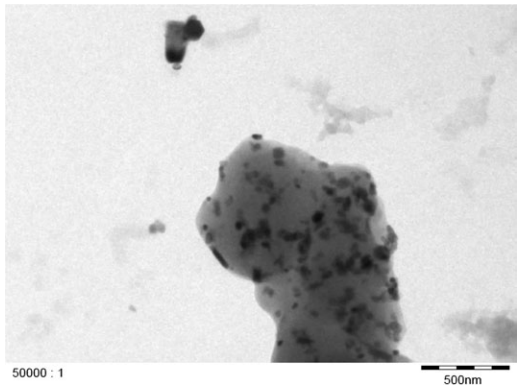

Fig. 11. TEM image of the generated wear from coating sample PU-ZnO; bar size 500 nm.

and 6.36×10^4 cm^{-3} will be generated by sanding the surface coatings. For the interpretation of the calculated concentrations, a comparison to urban aerosol measurements is possible. For example, in street canyons, the particle number concentration reaches from 2.5×10^4 cm^{-3} to 1.5×10^5 cm^{-3}; on weekdays, $>1.0 \times 10^5$ cm^{-3} was measured by Wehner *et al.* (2002).

CONCLUSION

A professional sanding process was simulated by operating a miniature sander at special process parameters to characterize the particle release from surface coatings with and without doped nanoparticles. The particle release in the nanometer range and above is quantified as the number of the released particles from a sanding area of 13 cm^2, at a contact pressure of 10 kPa, and at a relative peripheral speed of 1.83 m·s^{-1} using an abrasive paper with a graining of 600.

For the given stress, the swarf mass, the particle size distribution of the released aerosol, and consequently the number of released particles depend primarily on the used surface coating. First, results show a considerable generation of nanoparticles during the sanding process. However, no significant difference could be observed between coatings containing and not containing nanoparticle additives. This conclusion agrees with the results of Koponen *et al.* (2009) from the total particle emissions of a commercial hand-held sander. TEM images of precipitated swarf particles show that the generated nanoparticles are rather made up from matrix material, which contains the embedded additives.

Repeated measurement showed despite the reasonable spread of abraded swarf mass data, a large spread in the released particle numbers. The variation of the swarf mass results from random errors of only the abrasion process of material from the coating, whereas the variation of the total number of particles depend additionally on the random errors of the dispersion process of the abraded swarf material into air.

The measured nanoparticle releases would cause high nanoparticle concentrations in a model room of 3 m height, which are comparable to urban aerosols in street canyons. Because the aerosol was sampled directly in the neighborhood of the grinding tool, the measured particle numbers represent a maximum of possible values in a practical case. In practice, agglomeration in the vacuum exhaust system of the sanding machine and precipitation in its aerosol filter bag will reduce the particle numbers significantly.

In further analyses, more types of surface coatings and other nanocomposites will be investigated. Also, the whole life cycle of the employed coatings should be observed, including aging and weathering.

Acknowledgements—The authors wish to thank the German Paint Industry Association (VdL), Frankfurt am Main, Germany, for the financial support, Bayer Technology Services GmbH, Leverkusen, Germany, for TEM investigations, and Institut für Lacke und Farben e.V., Magdeburg, Germany, for the surface coatings sample preparation.

REFERENCES

Agarwal JK, Sem GJ. (1980) Continuous flow, single particle counting condensation nucleus counter. J Aerosol Sci; 11: 343–57.

Baron PA, Willeke K. (2001) Aerosol measurement—principles, techniques, and applications. New York: John Wiley and Sons ISBN 0 471 35636 0.

Bauer F, Sauerland V, Gläsel H-J *et al.* (2002) Preparation of scratch and abrasion resistant polymeric nanocomposites by monomer grafting onto nanoparticles, 3a—effect of filler particles and grafting agents. Macromol Mater Eng; 287: 546–52.

Biskos G, Reavell K, Collings N. (2005) Description and theoretical analysis of a differential mobility spectrometer. Aerosol Sci Technol; 39: 527–41.

Deutsches Institut für Normung. (1995) DIN EN ISO 2178:1995. Non-magnetic coatings on magnetic substrates—measurement of coating thickness—magnetic method. Berlin, Germany: Beuth Verlag.

Gail L, Hortig H-P. (2004) Reinraumtechnik. Berlin, Germany: Springer-Verlag ISBN 3 540 20542 X.

Gläsel H-J, Bauer F, Ernst H *et al*. (2000) Preparation of scratch and abrasion resistant polymeric nanocomposites by monomer grafting onto nanoparticles, 2a—characterization of radiation-cured polymeric nanocomposites. Macromol Chem Phys; 201: 2765–70.

Graskow BR. (2001) Design and development of a fast aerosol size spectrometer. Cambridge, UK: University of Cambridge.

Hinds WC. (1999) Aerosol technology—properties, behaviour, and measurement of airborne particles. New York: John Wiley and Sons. ISBN 0 471 19410 7.

Hsu L, Chein H. (2007) Evaluation of nanoparticle emission for TiO_2 nanopowder coating materials. J Nanopart Res; 9: 157–63.

Karn B, Kuiken T, Otto M. (2009) Nanotechnology and in situ remediation: a review of the benefits and potential risks. Environ Health Perspect; 117: 1823–31.

Koponen I, Jensen K, Schneider T. (2009) Sanding dust from nanoparticle-containing paints: physical characterisation. J Phys Conf Ser; 151. doi:10.1088/1742-6596/151/1/012048.

Lam C-W, James JT, McCluskey R *et al*. (2004) Pulmonary toxicity of single-wall carbon nanotubes in mice 7 and 90 days after intratracheal instillation. Toxicol Sci; 77: 126–34.

Mirme AA, Peil IA. (1983) A multichannel electrical aerosol spectrometer with a changeable measuring range and resolving power. Acta Commetat Univ Tartu; 648: 73–9.

Sem GJ. (2002) Design and performance characteristics of three continuous-flow condensation particle counters: a summary. Atmos Res; 62: 267–94.

Sepeur S, Kunze N, Werner B *et al*. (1999) UV curable hard coatings on plastics. Thin Solid Films; 351: 216–9.

Singh N, Manshian B, Jenkins G *et al*. (2009) Nanogenotoxicology: the DNA damaging potential of engineered nanomaterials. Biomaterials; 30: 3891–914.

Tammet H, Mirme AA, Tamm E. (2002) Electrical aerosol spectrometer of Tartu University. Atmos Res; 62: 315–24.

Thorpe A, Brown R. (1994) Measurement of the effectiveness of dust extraction systems of hand sanders used on wood. Ann Occup Hyg; 38: 279–302.

Vorbau M, Hillemann L, Stintz M. (2009) Method for the characterization of the abrasion induced nanoparticles release into air from surface coatings. J Aerosol Sci; 40: 209–17.

Wehner B, Birmili W, Gnauk T *et al*. (2002) Particle number size distributions in a street canyon and their transformation into the urban-air background: measurements and a simple model study. Atmos Environ; 36: 2215–23.